Calmodulin Regulation of Na$_V$1.4 Current: Role of Binding to the Carboxyl Terminus

Subrata Biswas, Isabelle Deschênes, Deborah DiSilvestre, Yanli Tian, Victoria L. Halperin, and Gordon F. Tomaselli

Department of Medicine, Division of Cardiology, Johns Hopkins University School of Medicine, Baltimore, MD 21205

Calmodulin (CaM) regulates steady-state inactivation of sodium currents (Na$_V$1.4) in skeletal muscle. Defects in Na current inactivation are associated with pathological muscle conditions such as myotonia and paralysis. The mechanisms of CaM modulation of expression and function of the Na channel are incompletely understood. A physical association between CaM and the intact C terminus of Na$_V$1.4 has not previously been demonstrated. FRET reveals channel conformation-independent association of CaM with the C terminus of Na$_V$1.4 (CT-Na$_V$1.4) in mammalian cells. Mutation of the Na$_V$1.4 CaM-binding IQ motif (Na$_V$1.4$_{IQ/AA}$) reduces cell surface expression of Na$_V$1.4 channels and eliminates CaM modulation of gating. Truncations of the CT that include the IQ region abolish Na current. Na$_V$1.4 channels with one CaM fused to the CT by variable length glycine linkers exhibit CaM modulation of gating only with linker lengths that allowed CaM to reach IQ region. Thus one CaM is sufficient to modulate Na current, and CaM acts as an ancillary subunit of Na$_V$1.4 channels that binds to the CT in a conformation-independent fashion, modulating the voltage dependence of inactivation and facilitating trafficking to the surface membrane.

INTRODUCTION

Voltage-gated sodium channels (Na$_v$) underlie the rising phase and influence the duration of action potentials in excitable cells such as neurons and cardiac and skeletal myocytes. Heritable defects in Na channel expression and gating are associated with myotonia (Yang et al., 1994; Wang et al., 2003; Wu et al., 2005), epilepsy (Kearney et al., 2001; Lossin et al., 2002), and sudden cardiac death (Keating and Sanguinetti, 2001). Na$_v$ currents are regulated by the ubiquitous calcium-sensing protein calmodulin (CaM). The carboxy terminus (CT) of these channels contains a CaM-binding, so-called IQ motif (Mori et al., 2000; Deschênes et al., 2002). The Na channel IQ motif is homologous to CaM binding sites in canonical CaM-regulated channels, such as L-type Ca channels, which are evolutionarily related to Na channels.

Despite the conservation of a CaM-binding IQ motif in all Na$_V$s, CaM regulation of Na currents is isoform specific (Deschênes et al., 2002; Herzog et al., 2003; Young and Caldwell, 2005). In vitro, cell-free association of CaM with the CT of Na$_V$ channels has been demonstrated; however, such studies could be compromised by nonphysiological CT peptide conformations that exist under conditions that are required to solubilize the channel or channel fragments. Moreover, there is little known about channel state dependence of CaM binding, the number of CaM molecules required to regulate

Na$_V$ inactivation, and effects on channel function other than gating. Here we explore whether CaM binds to the CT of intact Na$_V$1.4 channels and if this interaction is conformation specific. We fused enhanced fluorescence protein to the cytoplasmic C termini of Na$_V$1.4 and CaM; the interaction of CaM with Na$_V$1.4-CT was monitored using fluorescence resonance energy transfer (FRET) in live cells. The data reveal an intimate spatial relationship between CaM and the Na$_V$1.4 CT that is conformation independent. CaM interaction with the CT of Na$_V$1.4 influences trafficking of the channel protein to the surface membrane and modulates steady-state inactivation. The fusion of a single CaM molecule to the channel near the IQ through a glycine linker was sufficient to modulate Na$_V$1.4 gating, suggesting that a single CaM binding to the CT of Na$_V$1.4 is sufficient for modulation of inactivation.

MATERIALS AND METHODS

Plasmid Construction

EYFP/ECFP Fused to Wild Type and Mutant Sodium Channels.
DNA fragments containing EYFP and ECFP were prepared by the addition of an in-frame insert containing EYFP/ECFP. Na$_V$1.4 was cloned into the EcoR1 site of mammalian expression vector GW1H. The fragments were cloned in frame to the CT of Na$_V$1.4 to create Na$_V$1.4-ECFP/EYFP. The EYFP/ECFP fragments were generated by PCR amplification of regions of pEYFP/pECFP

Abbreviations used in this paper: CaM, calmodulin; CT, carboxy terminus; DIC, differential interference contrast; FRET, fluorescence resonance energy transfer; Na$_V$, voltage-gated sodium channel.

(CLONTECH Laboratories, Inc.) vectors encoding the fluorescent protein with primers that contain an NheI site in the forward primer (5′-AATGAACAGCTAGCGTACCGGTCGCCACCATGG) and NotI in the reverse primer (5′-TTCTAGAGTCGCGGCCGCTT for EYFP and 5′-TCTAGAGTCGCGGCCGGAA for ECFP). The stop codon of Nav1.4 was replaced with an NheI site, and the EYFP/ECFP fragments were directionally cloned into this site and a NotI site in the GW1H. The IQ/AA mutants (I1727A/Q1728A) were made by site-directed mutagenesis of the $Na_V1.4$-ECFP/EYFP construct.

Construction of $Na_V1.4$-ECFP/EYFP Deletion Mutants. Inserts containing the $Na_V1.4$ cDNA that were truncated at codons 1723 ($Na_V1.4_{1723}$) or 1740 ($Na_V1.4_{1740}$) in frame with either ECFP or EYFP, were generated by PCR using the forward primer $Na_V1.4$-BstZF (CTGCGTCAACACCACCACCT) and either one of the reverse primers $Na_V1.4$-1723NheR (1736bp) or $Na_V1.4$-1740NheR (1787 bp). The reverse primers used to prepare the 1723 and 1740 truncations were TCGAATCAGCTAGCACACACCTCCTCCTGCTTCC and TCGAATCAGCTAGCCACGGAGCGCTGCAGCAGG, respectively. The PCR products that generated the truncations were ligated into pGW1H-$Na_V1.4$ digested with BstZ17I and NheI. All the clones were sequence confirmed.

Construction of $Na_V1.4_{1740}$-Glycine-CaM-EYFP. Glycine (G$_4$)-linkered CaM was inserted into $Na_V1.4_{1740}$-EYFP by cloning a PCR product of full-length CaM flanked by in-frame Nhe1 sites into an NheI site between the channel and fluorescent protein coding regions. The G$_4$-CaM insert was prepared by PCR using a calmodulin-containing plasmid as template and the forward primer 5′-attcatGCTAGCGGAGGAGGCGGGATGGCTGACACTGA-3′ and the reverse primer 5′-attcatGCTAGCCTTCGCTGTCATCATTT-GTAC-3′. The forward primer contains an in-frame Nhe1 site followed by four glycine codons and then the calmodulin start sequence, the reverse primer contains an Nhe1 site and the end of the calmodulin coding region without the stop codon. The G$_4$ construct was used to prepare the construct with CaM linkered with 14 glycines (G$_{14}$). The linker length was increased from 4 to 14 glycines by mutation of the 5′ Nhe1 site to an AvrII site and the insertion of annealed oligonucleotides encoding 10 glycines and containing AvrII sticky ends.

Cell Culture and Transfection
Approximately 0.75×10^6 human embryonic kidney cells (HEK293; American Type Culture Collection) were cultured in six-well tissue dishes in DMEM supplemented with FBS 10%, L-glutamine (2 mmol/liter), penicillin (100 U/ml), and streptomycin (10 mg/ml). The cells were cotransfected with β1 and plasmids encoding wild-type sodium channels $Na_V1.4$-EYFP, $Na_v1.4$-ECFP or mutant $Na_V1.4_{IQ/AA}$-ECFP, $Na_V1.4_{IQ/AA}$-EYFP, $Na_V1.4_{1740}$-EYFP, $Na_V1.4_{1723}$-EYFP, and wild-type ECFP/EYFP-CaM or mutant ECFP/EYFP-CaM$_{1234}$ alone or in combination. Cells were transfected using Lipofectamine™ 2000 (Invitrogen) according to the manufacturer's instructions and were studied 48–72 h post-transfection. The total amount of DNA for all transfections was kept constant.

Electrophysiology
HEK293 cells expressing wild-type or mutant tagged $Na_V1.4$ channels and CaM or CaM$_{1234}$ were patch clamped with an Axopatch 200B patch-clamp amplifier using pipettes with tip resistances of 1–3 MΩ and typical series resistance compensation of >90% to minimize voltage clamp errors. Transfected cells were identified for patch clamping by ECFP, EYFP, or GFP fluorescence. Current recording was initiated 10 min after establishing the whole-cell configuration to avoid time-dependent shifts in gating. The bath solution contained (in mM) 150 NaCl, 2 KCl, 2 CaCl$_2$, 1 MgCl$_2$, 10 glucose, and 10 Na-HEPES (pH 7.4). The patch pipette contained (in mM) 35 NaCl, 3.7 CaCl$_2$, 5 BAPTA, and 10 Cs-HEPES (pH 7.3).

The free [Ca^{2+}] in the pipette was ∼0.5 μM; the bath and pipette solutions were adjusted to same osmolarity using glucose.

For simultaneous FRET measurements cells were held at −140, −60, and −20 mV during the collection of emitted light. A standard two-pulse protocol (500 ms pulse from −140 to −50 mV and a 50-ms test pulse to −20 mV) was used to generate the steady-state inactivation curves. Recovery from inactivation was assessed with a two-pulse protocol with a 30-ms first pulse to −20 mV followed by a variable interpulse interval and a second 30-ms pulse to assay recovery from predominantly fast inactivated states. Entry into inactivated states was assessed by a variable first test pulse to −20 mV (1–10,000 ms), followed by a 10-ms interpulse interval and a second test pulse of 50 ms to −20 mV to assay entry into slowly recovering (intermediate and slow) inactivated states.

FRET Measurements
Measurements of single-cell FRET based on aggregate (non-spatial) fluorescence recordings with donor dequenching were performed as previously described (Erickson et al., 2001) with minor modifications. Donor dequenching experiments were performed using a CFP filter cube (D440/20M (excitation), 455DCLP (dichroic), D480/30M (emission; Chroma Technology Corp.) before and 5 min after intense illumination using a custom YFP photobleaching cube (Chroma Technology Corp.), consisting of a D535/50× excitation filter and a 100% mirror (in place of a dichroic mirror). In control experiments this bleaching protocol spared CFP fluorescence. Epifluorescence images were acquired with a PI1300 CCD camera (Princeton Instruments) mounted to the side port of Olympus IX70 inverted microscope (60 × 1.4 objective; oil) driven by Metamorph software (Version7.0, Molecular Devices). The exposure time was set during the prebleach image acquisition and was not changed throughout the acquisition. Intensities were measured from a user-defined region of interest within the area of YFP fluorescence. Each image was background adjusted by subtracting the average pixel intensity from a region in the same field located outside the cell. Donor dequenching FRET efficiency (E_{EFF}) was calculated using a previously described method (Erickson et al., 2001) in SigmaPlot (Systat Software Inc.). Movies of cell fluorescence intensities were recorded by stream acquisition (600 frames, 50-ms exposure time). The CaM and $Na_V1.4$ interaction was further studied using the nondestructive 3^3 (three cube) FRET method, which has been previously used in CFP/YFP FRET to show interaction of CaM with the L-type Ca^{2+} channel. 3^3 FRET is highly concordant with donor dequenching FRET, thus is used as a complementary method to verify results of donor dequenching FRET. 3^3 FRET avoids the need for photolysis of the acceptor, thus reducing the possibility of artifactual changes in the quantum yield of the donor. The 3^3 method measures the FRET ratio, a fractional increase in YFP emission due to FRET, by eliminating direct excitation of YFP and contaminating CFP emission using different filter cubes. 3^3 FRET images were acquired with the following filter cubes (excitation, dichroic, emission): CFP filter cube (D440/20M, 455DCLP, D480/30M, Chroma Technology Corp.); the YFP filter cube (HQ500/20×, Q515LP, HQ505/30, Chroma Technology Corp.); and the FRET filter cube (D440/20M, Chroma Technology Corp.), 455DRLP (Omega Optical Inc. Brattleboro, VT), HQ535/30 (Chroma). The FRET ratio and FRET efficiency were calculated as previously described (Erickson et al. 2001).

Cell Surface Expression and Western Blot Analysis
The cells were cotransfected with equal amounts (0.5 μg/ml) of either wild-type $Na_V1.4$-EYFP or $Na_V1.4_{1740}$-EYFP or $Na_V1.4_{IQ/AA}$-EYFP plasmids. The concentrations of plasmids were estimated spectrophotometrically and further confirmed by agarose gel electrophoresis (not depicted). The cells were grown to a similar level of confluence and then surface channels were biotinylated and

TABLE I

Effect of CaM and CaM$_{1234}$ Overexpression on Na$_V$1.4, Na$_V$1.4-EYFP and Na$_V$1.4$_{1740}$-EYFP

Channel/Mutant	V$_{1/2}$ steady state inactivation	Decay time constant τ$_h$	V$_{1/2}$ activation	Current density
	mV	*ms at −20 mV*	*mV*	*pA/pF*
Na$_V$1.4-EYFP + β1	−65.2 ± 0.4 (n = 5)	0.69 ± 0.04	−32.2 ± 0.1	−426.4 ± 93.3
Na$_V$1.4-EYFP + ECFP-CaM + β1	−71 ± 0.2 (n = 5)	0.77 ± 0.05	−32.6 ± 0.2	−458.0 ± 54.0
Na$_V$1.4-EYFP + ECFP-CaM$_{1234}$ + β1	−64.2 ± 0.1 (n = 5)	0.66 ± 0.02	−32.9 ± 0.1	−269.6 ± 55.5
Na$_V$1.4 + β1	−65.08 ± 0.1 (n = 6)	0.61 ± 0.07	−32.1 ± 0.3	−453.2 ± 71.5
Na$_V$1.4 + ECFP-CaM + β1	−69.3 ± 0.1 (n = 7)	0.63 ± 0.02	−30.6 ± 0.2	−309.4 ± 112.0
Na$_V$1.4 + ECFP-CaM$_{1234}$ + β1	−64.3 ± 0.3 (n = 7)	0.66 ± 0.07	−31.2 ± 0.1	−324.1 ± 80.9
Na$_V$1.4$_{IQ/AA}$ + β1	−79.4 ± 0.2 (n = 6)	1.3 ± 0.2	−40.9 ± 0.3	−307.8 ± 89.9
Na$_V$1.4$_{IQ/AA}$ + ECFP-CaM + β1	−80.0 ± 0.4 (n = 6)	1.25 ± 0.15	−40.0 ± 0.1	−242.5 ± 60.5
Na$_V$1.4$_{IQ/AA}$ + ECFP-CaM$_{1234}$ + β1	−80.7 ± 0.3 (n =5)	1.12 ± 0.15	−41.0 ± 0.3	−254.2 ± 73.1
Na$_V$1.4$_{1740}$ + β1	−62.7 ± 0.1 (n = 6)	0.69 ± 0.09	−30.1 ± 0.2	−437.8 ± 116.0
Na$_V$1.4$_{1740}$ + ECFP-CaM + β1	−68.0 ± 0.1 (n = 8)	0.62 ± 0.02	−29.5 ± 0.1	−294.0 ± 74.7
Na$_V$1.4$_{1740}$ + ECFP-CaM$_{1234}$ + β1	−64.0 ± 0.04 (n = 5)	0.79 ± 0.01	−31.1 ± 0.2	−295.0 ± 60.9
Na$_V$1.4$_{1740}$-G4-CaM + β1	−65.8 ± 0.1 (n = 8)	0.69 ± 0.09	−30.8 ± 0.3	−372.9 ± 67.4
Na$_V$1.4$_{1740}$-G4-CaM + ECFP-CaM + β1	−71.4 ± 0.2 (n = 9)	0.55 ± 0.3	−30.7 ± 0.1	−373.0 ± 77.5
Na$_V$1.4$_{1740}$-G4-CaM + ECFP-CaM$_{1234}$ + β1	−63.6 ± 0.2 (n = 5)	0.52 ± 0.1	−32.1 ± 0.2	−413.5 ± 118.9
Na$_V$1.4$_{1740}$-G14-CaM + β1	−68.4 ± 0.2 (n = 9)	0.60 ± 0.1	−31.9 ± 0.3	−201.4 ± 63.2
Na$_V$1.4$_{1740}$-G14-CaM + ECFP-CaM + β1	−67.7 ± 0.2 (n = 9)	0.51 ± 0.06	−30.2 ± 0.3	−391.5 ± 121.1
Na$_V$1.4$_{1740}$-G14-CaM + ECFP-CaM$_{1234}$ + β1	−66.7 + 0.1 (n = 9)	0.53 ± 0.06	−32.0 ± 0.1	−439.5 ± 141.9

total cell lysates were isolated; this includes biotin-labeled (cell surface) and unlabeled channels (the remainder). HEK293 cells were surface biotinylated for 1 h at 4°C using Sulfo-NHS-SS-Biotin (Pierce Biotechnology Inc.) 48 h after transfection. After quenching the excess biotin, cells were washed and lysed in 500 μl of 2% SDS, 50 mM EDTA with brief probe sonication. The total cell lysate was aliquoted and a fraction was used for purification of biotinylated proteins using Immobilized NeutrAvidin (Pierce Biotechnology Inc.) according to the manufacturer's protocol. The same volumes of total cell lysate and NeutrAvidin precipitates were run on the same SDS-PAGE (7%) gels, transferred to nitrocellulose membranes, and incubated with a monoclonal anti-Na channel antibody (Sigma-Aldrich, IgG$_1$ anti-mouse 1:500). The intensities of bands on the Western blots were quantified using Metamorph software (Version7.0, Molecular Device). The density of the biotinylated protein bands were normalized to their respective total lysate densities from the same gels. The intensity ratios (biotinylated proteins/total lysate proteins) were compared for each of the Na channel α subunit variants expressed in the absence of CaM. For detection of CaM, HEK293 cells were transfected with ECFP-CaM (gift from D.T. Yue, Johns Hopkins University), ECFP-CaM$_{1234}$, or ECFP alone (1 μg/ml). 48 h after transfection cells were lysed, briefly probe sonicated and proteins from the same volume of cell lysates were separated and analyzed by Western blotting with anti-CaM and anti-GFP antibodies (Covance).

Confocal microscopy

Approximately 0.75×10^6 cells were plated and then transfected on coverslips in a six-well culture dish fixed in 4% formaldehyde 48 h after transfection. Fixed HEK293 cells expressing Na$_V$1.4-EYFP or the IQ mutant Na$_V$1.4$_{IQ/AA}$-EYFP fusion proteins were imaged using a confocal microscope (LSM510, Carl Zeiss Micro-Imaging, Inc.) with 63×/1.4 or 100×/1.4 oil differential interference contrast (DIC) plan apochromat objectives (Carl Zeiss Micro-Imaging, Inc.). EYFP was excited at 514 nm with an LSM510 Argon laser and emitted light was detected with a 530–600-nm band pass filter and beam splitter (HFT 405/514, mirror and NFT 515). Transmitted DIC images were obtained simultaneously.

Data Analysis

Electrophysiological, protein expression, and FRET data were expressed as the means ± SEM and inactivation data were fit to a Boltzmann function. Data for entry into inactivation and recovery from inactivation were fit to exponential functions. Significance was assessed using a t test (Microcal Origin, Microcal Software Inc.).

Online Supplemental Material

The online supplemental material (available at http://www.jgp.org/cgi/content/full/jgp.200709863/DC1) contains two figures. Fig. S1 summarizes the biophysical properties of Na$_V$1.4$_{IQ/AA}$ in the presence of CaM and AIP. Fig. S2 illustrates the effect of the C-terminal truncation Na$_V$1.4$_{1723}$ on channel trafficking by epifluorescence microscopy and Western blotting.

RESULTS

CT-Na$_V$1.4 Fusion Constructs Are Functionally Expressed and Interact with CaM

We have previously shown that CaM associates with wild type GST-tagged Na$_V$ CT peptides in vitro (Deschênes et al., 2002), this work motivated studies of the interaction between the CT of intact Na$_V$ channels and CaM in live cells using FRET. We designed channel fusions with fluorescent proteins linked to the CT, which is close in the linear amino acid sequence to the IQ motif, optimizing the possibility of FRET detection on CaM binding. One of the major concerns about fusion of a fluorophore to CT is the possibility of functional alterations of the sodium current by tagging the channel. The CT EYFP/ECFP-tagged Na$_V$1.4 channels were fully characterized and did not exhibit significant changes in current–voltage relationship or the voltage dependence of activation and steady-state inactivation compared
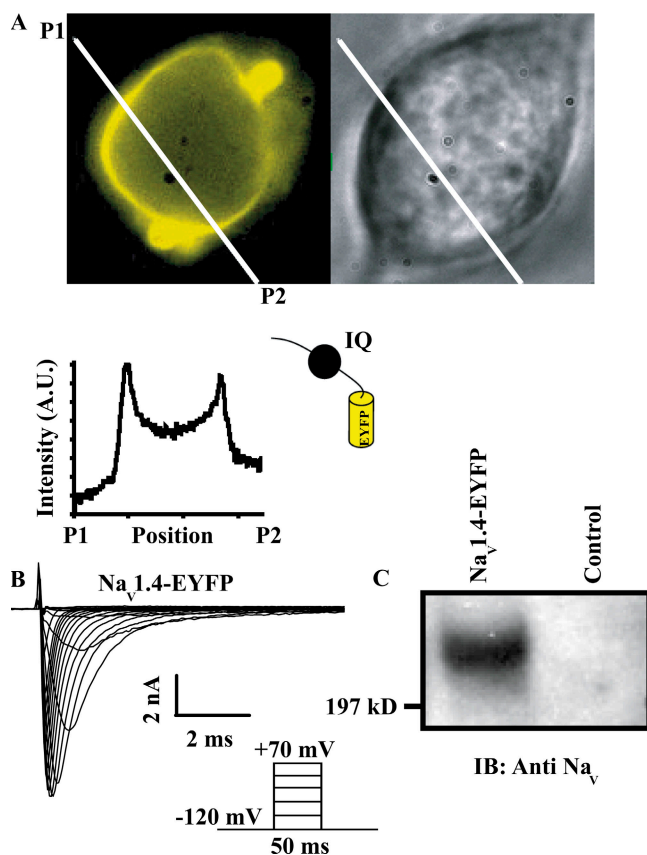
Figure 1. Na$_V$1.4-EYFP expression. (A) Na$_V$1.4-EYFP expression in HEK293 cells. Epifluoresecence image and intensity profile of an HEK293 cell expressing Na$_V$1.4-EYFP and Na$_V\beta$1subunits. The peaks in the fluorescence profiles indicate membrane targeting. (B) A family of Na$_V$1.4-EYFP currents elicited by the voltage protocol shown in the inset. (C) Western blot of total cell lysates from Na$_V$1.4-EYFP–transfected (1 μg/ml) HEK293 cells and nontransfected controls. Lysates isolated 48 h after transfection, separated by Western blot, and probed with an anti-Na$_V$ antibody exhibit a band near 197 kD representing Na$_V$1.4-EYFP expression.

with untagged wild-type channels expressed in HEK293 cells (Table I).

The channel fusion constructs expressed in HEK293 cells display a distinct fluorescent enrichment at the cell perimeter consistent with surface membrane expression (Fig. 1 A). Cells transfected with Na$_V$1.4-EYFP express robust currents (Fig. 1 B) that are indistinguishable from untagged wild-type Na$_V$1.4 (Table I), confirming that labeled channels are functional and targeted to the membrane. Western blots of lysates from cells transfected with Na$_V$1.4-ECFP or -EYFP reveal a band of ∼225 kD, consistent with the expression of labeled channels (Fig. 1 C).

In contrast to channel expression, ECFP-CaM expression or the EF hand mutant of CaM (ECFP-CaM$_{1234}$) alone in HEK293 cells is uniform throughout the cell (Fig. 2 A; ECFP-CaM$_{1234}$ not depicted). Western blots from cells transfected with ECFP-CaM or
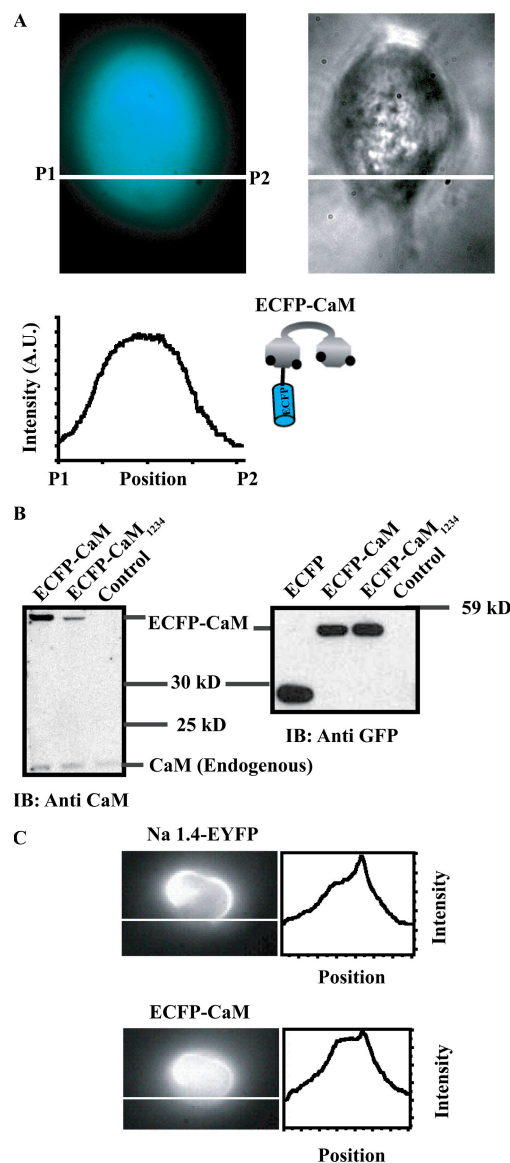

Figure 2. ECFP-CaM overexpression in HEK293 cells. (A) Epifluorescence image and intensity profile of an HEK293 cell expressing ECFP-CaM alone shows uniform cytosolic expression of CaM. (B) Immunoblot of HEK293 lysates probed with an anti-CaM antibody demonstrates endogenous CaM, ECFP-CaM, and ECFP-CaM$_{1234}$ (left). Immunoreactive ECFP, ECFP-CaM, and ECFP-CaM$_{1234}$ are shown with an anti-GFP antibody. (C) Epifluoresecence image and intensity profile of Na$_V$1.4-EYFP coexpressed with ECFP-CaM in HEK293 cells; the peaks indicate membrane targeting. In the top panel, the cell is excited with 535-nm light and the bottom panel is the same cell excited with 440-nm light showing enrichment of ECFP-CaM at the cell membrane when coexpressed with Na$_V$1.4-EYFP.

ECFP-CaM$_{1234}$ exhibit distinct bands representing labeled CaM and CaM$_{1234}$, which can be distinguished from either ECFP or endogenous native CaM expression (Fig. 2 B). The levels of endogenous CaM are comparable to that of fluorophore-conjugated CaM in Western blots (Fig. 2 B). Thus, analysis based on single-cell voltage clamp recording and fluorescence microscopy
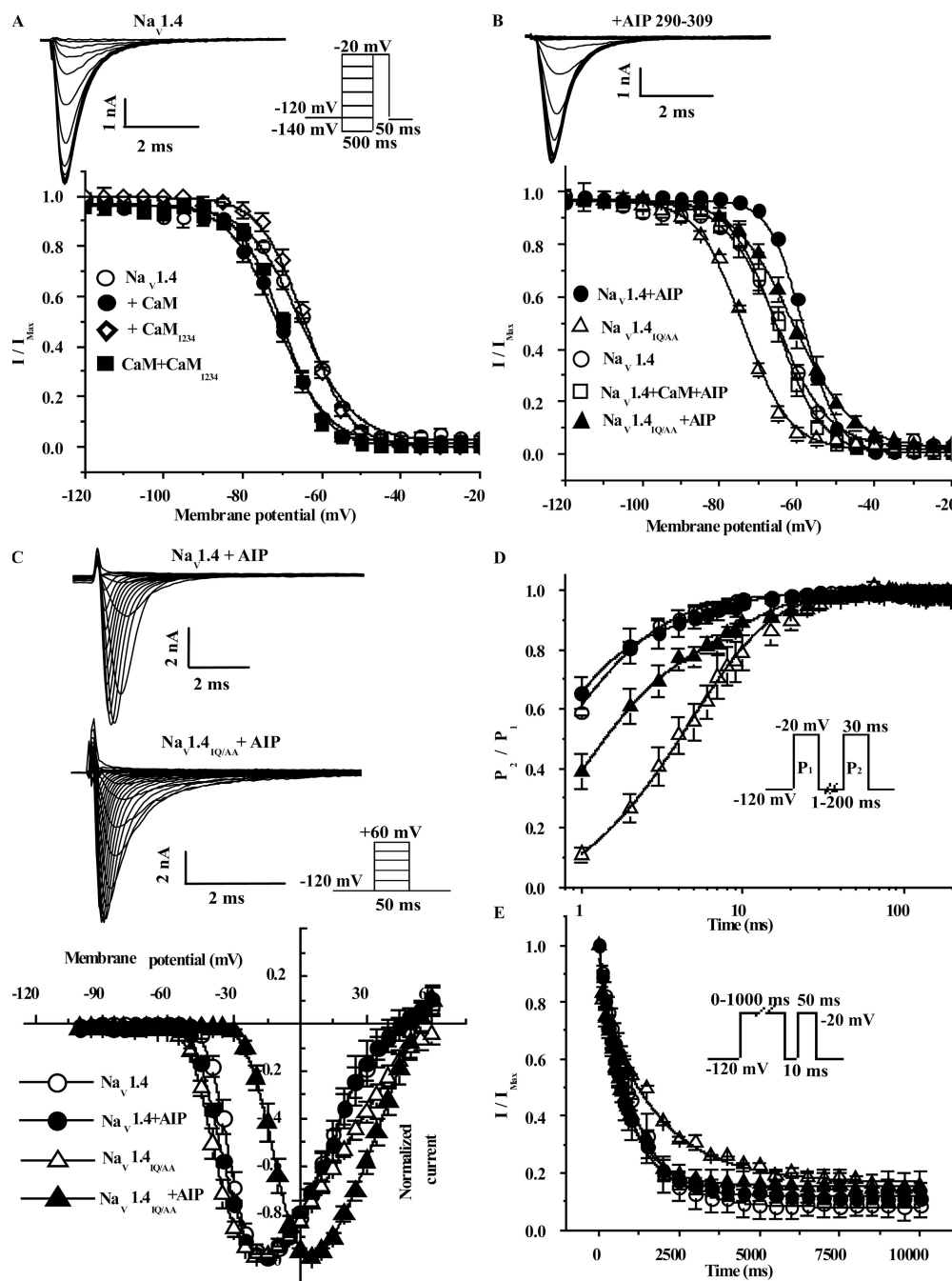
Figure 3. CaM modulation of inactivation gating of $Na_V1.4$. (A) A representative family of $Na_V1.4$-EYFP currents elicited by the steady-state inactivation protocol shown in the inset. Currents were recorded at a test pulse of -20 mV after a 500-ms conditioning pulse from -140 to $+30$ mV. The bottom panel shows the steady-state inactivation curves of $Na_V1.4$ EYFP expressed in HEK293 cells alone ($\bigcirc$) or coexpressed with ECFP-CaM ($\bullet$) or ECFP-CaM$_{1234}$($\diamond$), and in the presence of both ECFP-CaM and EYFP-CaM$_{1234}$ ($\blacksquare$). The data are means ± SEM and fit to Boltzmann function. (B) A representative family of $Na_V1.4$-EYFP currents in the presence of AIP290-309 elicited by the steady-state inactivation protocol in (A). The CaM antipeptide AIP290-309 added to the pipette solution abolishes the CaM-induced shift in the steady-state inactivation of $Na_V1.4$-EYFP ($\square$), AIP290-309 in the absence of overexpression of CaM induces a rightward shift in the $V_{1/2}$ of steady-state inactivation ($\bullet$). In IQ/AA mutant channels, AIP290-309 induces a rightward shift in the $V_{1/2}$ of steady-state inactivation of $Na_V1.4_{IQ/AA}$-EYFP ($\blacktriangle$) compared with the absence of AIP290-309 ($\triangle$). (C) Effect of AIP290-309 on the normalized current–voltage relationships of $Na_V1.4_{IQ/AA}$-EYFP and $Na_V1.4$-EYFP currents. The top panels are representative raw current records of $Na_V1.4$ and mutant $Na_V1.4_{IQ/AA}$ channels with AIP290-309 (protocol in the inset). The normalized current–voltage (IV) relationships for $Na_V1.4$-EYFP in absence ($\bigcirc$) and presence of AIP290-309 ($\bullet$), and for $Na_V1.4_{IQ/AA}$-EYFP ($\triangle$) reveal that peak IV relationship for $Na_V1.4_{IQ/AA}$ is significantly shifted in the depolarizing direction in presence of AIP290-309 ($\blacktriangle$). (D) The recovery of the channels from inactivation measured using the protocol in the inset reveal that τ_{rec} of $Na_V1.4_{IQ/AA}$ in presence of AIP290-309 ($\blacktriangle$) is significantly shorter than that of $Na_V1.4_{IQ/AA}$ in the absence of AIP290-309 ($\triangle$). The τ_{rec} of $Na_V1.4$ is not significantly different in the absence ($\bigcirc$) and presence of AIP290-309 ($\bullet$). (E) The entry of the channels into inactivation was measured using the protocol in the inset. The τ_{entry} of $Na_V1.4_{IQ/AA}$ is decreased in the presence of AIP290-309($\blacktriangle$), the τ_{entry} of $Na_V1.4$ ($\bullet$) in the presence of AIP290-309 is not significantly different from $Na_V1.4$ in the absence of AIP290-309($\bigcirc$).

is necessary to evaluate the effect of overexpressed CaM. If CaM is associated with $Na_V1.4$, one would predict enrichment of CaM at the cell membrane based on the distribution of $Na_V1.4$ in the surface membrane (Fig. 1 A). Cells expressing both labeled channels and ECFP-CaM show a small peak in the image profile cor-

responding to surface membrane enrichment of ECFP-CaM (Fig. 2 C).

We characterized $Na_V1.4$-EYFP currents in the presence and absence of overexpressed ECFP-CaM and its EF hand mutant ECFP-CaM$_{1234}$. The currents generated by expression of the EYFP-fused channel construct
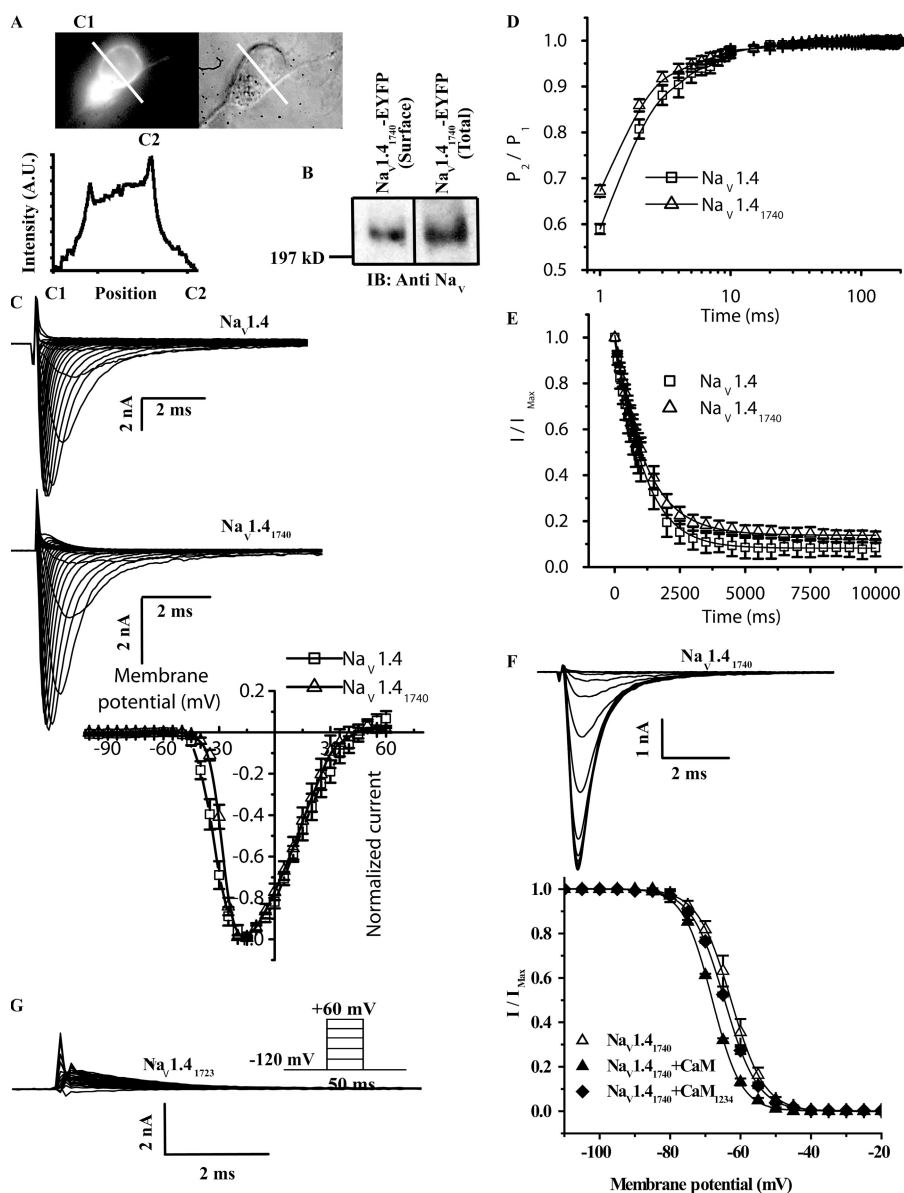
Figure 4. $Na_V1.4_{1740}$-EYFP preserves CaM-dependent modulation of steady-state inactivation. (A) Epifluoresecence image and intensity profile of $Na_V1.4_{1740}$-EYFP expressed with $Na_V\beta1$ in an HEK293 cell; the peaks indicate membrane targeting. (B) A Western blot of biotinylated surface proteins purified with streptavidin and probed with an anti-Na_V antibody (left lane). Total channel proteins are cell lysates that include biotin-labeled (cell surface) and unlabeled channels (the remainder) (right lane). The deletion mutant channel runs just above 197 kD. (C, left) Representative families of $Na_V1.4$-EYFP and $Na_V1.4_{1740}$-EYFP currents are similar. (bottom) The normalized IV relationships for $Na_V1.4$-EYFP ($\square$) and $Na_V1.4_{1740}$-EYFP ($\triangle$) are not significantly different. (D) Recovery from inactivation of $Na_V1.4_{1740}$-EYFP ($\triangle$) and $Na_V1.4$-EYFP ($\square$) are not significantly different. (E) Entry into inactivation of $Na_V1.4_{1740}$-EYFP ($\triangle$) and $Na_V1.4$-EYFP ($\square$) are not significantly different. (F) The steady-state inactivation curve of $Na_V1.4_{1740}$-EYFP ($\triangle$) is shifted in the hyperpolarizing direction by ECFP-CaM ($\blacktriangle$) but not by ECFP-CaM$_{1234}$ ($\blacklozenge$). (G) A truncation of the CT including the IQ region, $Na_V1.4_{1723}$-EYFP, eliminates channel function. The data expressed as the means ± SEM and inactivation data are fit to a Boltzmann function.

have activation and inactivation kinetics and peak amplitudes that were not different from the wild-type $Na_V1.4$ channel (Table I). The voltage dependence of steady-state inactivation was not altered by fusion of EYFP at the CT of $Na_V1.4$ (Fig. 3 A; Table I). The $V_{1/2}$ of steady-state inactivation of $Na_V1.4$-EYFP is -65.2 ± 0.4 mV ($n = 5$), coexpression of ECFP-CaM significantly ($P < 0.04$) shifts the $V_{1/2}$ ~5 mV ($V_{1/2} = -71 \pm 0.2$, $n = 5$) in the hyperpolarizing direction compared with $Na_V1.4$-EYFP expressed alone (Fig. 3 A). The voltage dependence of activation of the $Na_V1.4$-EYFP expressed in HEK293 cells ($V_{1/2} = -32.2 \pm 0.1$ mV, $n = 5$) was not altered by overexpression of CaM ($V_{1/2} = -32.6 \pm 0.2$ mV; $n = 5$) or CaM$_{1234}$ ($V_{1/2} = -32.9 \pm 0.1$ mV, $n = 5$) (Table I). Thus fusion of ECFP/EYFP to CT of $Na_V1.4$ and CaM does not alter the CaM-induced steady-state inactivation shift.

CaM Is Tethered to CT-$Na_V1.4$

We next asked if CaM or apo-CaM is tethered to the CT of intact $Na_V1.4$ channels and if there are alternate apo-CaM binding site(s) with functional effects on the Na current as in the L-type Ca^{2+} channel (Erickson et al., 2001, 2003). Overexpression of ECFP-CaM$_{1234}$ with $Na_V1.4$ does not shift the channel availability curve compared with $Na_V1.4$ expression alone in the presence of endogenous CaM (Fig. 3 A). These data indicate that apo-CaM does not affect steady-state inactivated channel availability; however, it does not exclude the possibility of apo-CaM binding to the channel. Overexpressing both wild-type EYFP-CaM and ECFP-CaM$_{1234}$ with $Na_V1.4$ produced no significant shift in the voltage dependence of the steady-state availability (Fig. 3 A; $V_{1/2} = -69.3 \pm 0.6$ mV, $n = 10$) compared with ECFP-CaM overexpression alone, suggesting the possibility that CaM may be
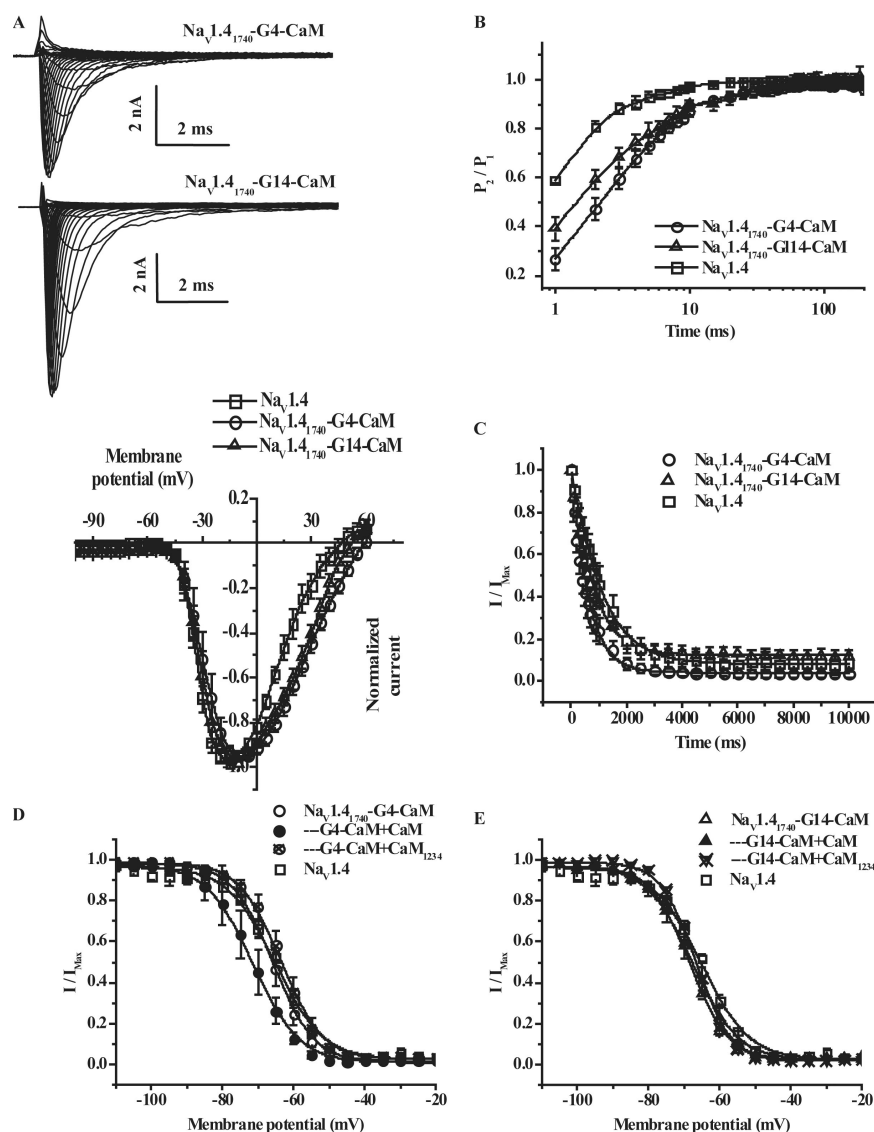
Figure 5. Properties of $Na_V1.4_{1740}$-glycine-CaM. (A) Representative raw current records of truncated $Na_V1.4$ channels with CaM linked to the CT by 4 (top, $Na_V1.4_{1740}$–G4–CaM) or 14 (bottom, $Na_V1.4_{1740}$–G14–CaM) glycine residues. The IV relationships reveal no significant differences between the channels linked to CaM and wild-type $Na_V1.4$ (right). (B) Recovery from inactivation of $Na_V1.4_{1740}$–G4–CaM (○) and $Na_V1.4_{1740}$–G14–CaM (△) are slower than that of wild-type, full-length $Na_V1.4$ (□). (C) The rates of entry into inactivated states are similar in $Na_V1.4_{1740}$–G4–CaM (○), $Na_V1.4_{1740}$–G14–CaM (△), and wild-type $Na_V1.4$ (□) channels. (D) Overexpression of wild-type CaM (●) but not CaM_{1234} (⊗) shifts the steady-state inactivation curve in the hyperpolarizing direction compared with $Na_V1.4_{1740}$–G4–CaM (○) or wild-type $Na_V1.4$ (□) expressed alone. (E) The steady-state inactivation curve of $Na_V1.4_{1740}$–G14–CaM (△) is unaffected by overexpression of CaM (▲) or CaM_{1234} (✗).

durably tethered to CT-$Na_V1.4$ and that apo-CaM does not displace CaM binding.

Inclusion of the CaM anti-peptide (AIP290-309) in the pipette solution mitigates the CaM-induced shift in the steady-state inactivation curve ($V_{1/2} = -63.7 \pm 0.2$ mV, $n = 7$) in cells coexpressing $Na_V1.4$- EYFP and ECFP-CaM (Fig. 3 B). These data are consistent with the peptide effectively competing with CaM binding to the CT of $Na_V1.4$ and supports the hypothesis that CaM binding to the CT is essential for modulation of the voltage dependence of inactivation gating. In the absence of CaM overexpression, AIP290-309 induced a +7-mV shift in the steady-state inactivation curve ($V_{1/2} = -58.5 \pm 0.2$ mV, $n = 7$) compared with cells expressing only $Na_V1.4$-EYFP (Fig. 3 B). AIP290-309 may be acting by displacement of endogenous CaM from the channel or through inhibition of CaM binding to other sites on $Na_V1.4$ or other effector proteins. However, in cells expressing $Na_V1.4_{IQ/AA}$, AIP290-309 induces an ~+12-mV

shift in the steady-state inactivation curve ($V_{1/2} = -61.1 \pm 0.1$ mV, $n = 10$) compared with cells expressing $Na_V1.4_{IQ/AA}$ in the absence of AIP ($V_{1/2} = -73.9 \pm 0.2$ mV, $n = 7$; Fig. 3 B). AIP290-309 has several distinct effects on gating of $Na_V1.4_{IQ/AA}$ that are not observed in the wild-type channel. AIP290-309 shifts the peak current–voltage relationship to right in $Na_V1.4_{IQ/AA}$ (Fig. 3 C). Channel recovery from inactivated states and entry into slowly recovering inactivated states were evaluated using the pulse protocols in the insets of Fig. 3, D and E, respectively. AIP hastens recovery (τ_{rec}) from fast inactivation state in IQ/AA mutant channels without affecting the wild-type channel (Fig. 3 D). AIP290-309 significantly reduces τ_{rec} from 5.5 ± 0.1 ms ($n = 7$) to 4.5 ± 0.7 ms in $Na_V1.4_{IQ/AA}$ ($n = 10$, Fig. 3 D) and decreases τ_{entry} from 1592.80 ± 127.4 ms ($n = 6$) to 815.3 ± 98.2 ms ($n = 7$, Fig. 3 E). In contrast, AIP290-309 did not significantly alter τ_{rec} or τ_{entry} of wild-type $Na_V1.4$ (Fig. 3, D and E). Thus the IQ/AA mutation

A

ECFP

ECFP + EYFP

ECFP-EYFP

ECFP + Na$_V$1.4-EYFP

ECFP-CaM + Na$_V$1.4$_{IQ/AA}$-EYFP

ECFP-CaM$_{1234}$ + Na$_V$1.4-EYFP

ECFP-CaM + Na$_V$1.4-EYFP

-15 -10 -5 0 5 10 15 20 25 30
%FRET Efficiency

B

ECFP + Na$_V$1.4-EYFP

ECFP-CaM + Na$_V$1.4$_{IQ/AA}$-EYFP

ECFP-CaM$_{1234}$ + Na$_V$1.4-EYFP

ECFP-CaM + Na$_V$1.4-EYFP

-500 -400 -300 -200 -100 0
pA / pF

C

FRET Efficiency (%)
0   9.8

ECFP-CaM$_{1234}$+Na$_V$1.4-EYFP

ECFP-CaM+Na$_V$1.4$_{IQ/AA}$-EYFP

ECFP-CaM + Na$_V$1.4-EYFP

0   1   2
FRET Ratio (A.U.)

D

ECFP-CaM + Na$_V$1.4-EYFP

-20

-60

-140
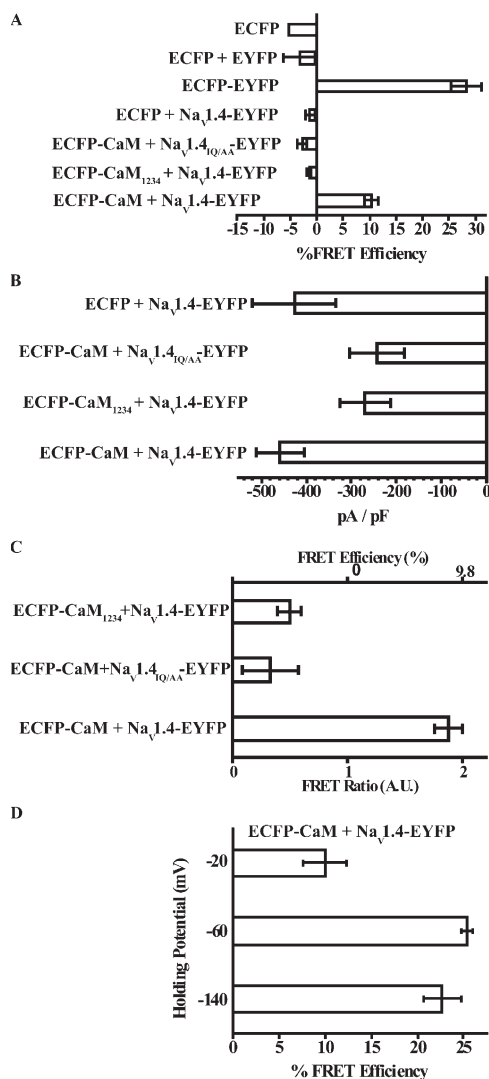
0   5   10   15   20   25
% FRET Efficiency

Figure 6. In vivo association of CaM with CT-Na$_V$1.4 by FRET. (A) Donor dequenching FRET in live HEK293 cells expressing the indicated channel constructs. The top three bars in the graph are the FRET efficiencies of control experiments in cells not expressing channels, but expressing ECFP alone, ECFP and EYFP, or the linked chameleon (ECFP-EYFP). Na$_V$1.4-EYFP coexpressed with ECFP or ECFP-CaM$_{1234}$, or Na$_V$1.4$_{IQ/AA}$ coexpressed with ECFP-CaM yield no detectible FRET. Na$_V$1.4-EYFP coexpressed with ECFP-CaM exhibits significant FRET (>5% efficiency). (B) Peak current densities of expressed Na$_V$1.4 and Na$_V$1.4$_{IQ/AA}$ channels used for FRET measurements. The densities of Na$_V$1.4-EYFP coexpressed with ECFP-CaM or ECFP-CaM$_{1234}$, or Na$_V$1.4$_{IQ/AA}$ coexpressed with ECFP-CaM are not significantly different from the current density of Na$_V$1.4-EYFP coexpressed with ECFP alone. (C) Interaction of CaM and Na$_V$1.4 assayed by the 3^3 FRET method. This nondestructive technique confirms the proximity of the fluorophores and the production of FRET in cells expressing Na$_V$1.4-EYFP and ECFP-CaM by a FRET ratio of almost 2. (D) Cells coexpressing Na$_V$1.4-EYFP and ECFP-CaM are held at different membrane voltages to populate different channel conformations. FRET is comparable in cells held at −140 and −60 mV, and is present but reduced at a holding voltage of −20 mV.

unmasks effects of AIP290-309 that are independent of CaM binding to the channel.

To further elucidate role of the IQ region in CaM binding and channel function, we studied deletion mutants with and without the IQ motif of the Na$_V$1.4 CT region. Deletion mutations of the Na$_V$1.4 CT that preserve the IQ motif (e.g., Na$_V$1.4$_{1740}$-EYFP) expressed in HEK293 cells display fluorescence enrichment at the cell perimeter. Line scans of fluorescence intensity are consistent with surface membrane expression of this truncation mutant (Fig. 4 A). Further qualitative analysis of Western blots of purified biotinylated Na$_V$1.4$_{1740}$ protein demonstrates expression of the truncated channels at the surface membrane (Fig. 4 B). The family of currents elicited by voltage-clamp pulses of the deletion mutant Na$_V$1.4$_{1740}$ is similar to intact Na$_V$1.4 (Fig. 4 C). The normalized current–voltage (Fig. 4 C) relationships of the Na$_V$1.4$_{1740}$ mutant and wild-type channels are nearly identical with the peak current amplitudes at −20 mV. τ_{rec} from fast inactivation of truncated channel is 1.7 ± 0.1 ms ($n = 5$), not significantly different from wild-type channel (1.9 ± 0.1 ms, $n = 5$; Fig. 4 D). Similarly, truncation of the nonstructured part of CT in Na$_V$1.4 distal to the IQ region does not significantly alter τ_{entry} (1165 ± 17 ms, $n = 6$), compared with the wild-type channel (1088 ± 20 ms, $n = 5$; Fig. 4 E). The steady-state inactivation curve of Na$_V$1.4$_{1740}$ reveals a V$_{1/2}$ of −62.7 ± 0.1 mV ($n = 6$) and coexpression of ECFP-CaM with Na$_V$1.4$_{1740}$ shifts the V$_{1/2}$ ∼5 mV (V$_{1/2}$ = −68.0 ± 0.1 mV, $n = 8$, P < 0.04) in the hyperpolarizing direction (Fig. 4 F). Overexpression of ECFP-CaM$_{1234}$ with Na$_V$1.4$_{1740}$ does not shift the availability curve compared with Na$_V$1.4$_{1740}$ expression alone (−64.6 ± 0.04 mV, $n = 5$; Fig. 4 F). Thus the deletion mutant Na$_V$1.4$_{1740}$ retains the basic biophysical properties of Na$_V$1.4 channels and CaM-induced modulation of steady-state inactivation (Table I). These data suggest that the nonstructured distal portion of the CT (after amino acid 1740) is not critical for modulation of channel gating by CaM. In contrast, deletion after amino acid 1723, which includes the entire nonstructured region and the IQ motif of CT-Na$_V$1.4 (Na$_V$1.4$_{1723}$), generated no current (Fig. 4 G). Thus the region containing the IQ motif in Na$_V$1.4 is essential to functional expression of the channel.

To define the mechanisms of CaM modulation of Na$_V$1.4 current we sought to determine the number of CaM molecules required for the channel modulation. We created a channel with CaM fused to the CT of Na$_V$1.4$_{1740}$ through variable length glycine linkers to promote the association of CaM with the channel from the earliest stages of biosynthesis and to increase the local concentration of CaM in the vicinity of IQ motif. Two different lengths of glycine linkers were used to tether CaM to the channel, short (4 glycines, Na$_V$1.4$_{1740}$–G4–CaM) and longer (14 glycines, Na$_V$1.4$_{1740}$–G14–CaM). The short linker does not permit CaM to have access to

A

Na$_V$1.4$_{IQ/AA}$(Total)	−	−	+	−
Na$_V$1.4 (Total)	−	−	−	+
Na$_V$1.4$_{IQ/AA}$(Surface)	+	−	−	−
Na$_V$1.4 (Surface)	−	+	−	−

197 kD ➤

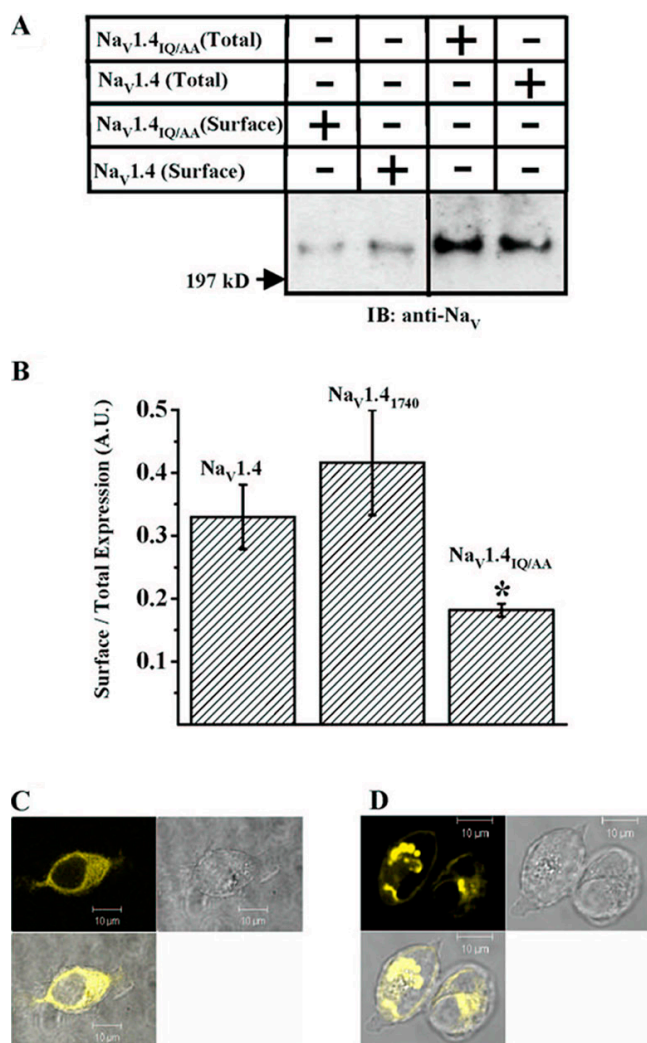IB: anti-Na$_V$

B

C

D

Figure 7. Influence of CaM on Na$_V$1.4 channel expression and localization. (A) Western blots of lysates from HEK293 cells transfected with wild-type Na$_V$1.4 and mutant Na$_V$1.4$_{IQ/AA}$ channels reveal a reduction in surface expression of Na$_V$1.4 protein by the IQ/AA mutation compared with wild type with no significant change in immunoreactive protein in total cell lysates. The protein is detected with the antibodies described in Fig. 1. (B) The ratio of cell surface expression to total expression of Na$_V$1.4$_{IQ/AA}$ is significantly (P ≤ 0.05, $n = 4$) reduced compared with wild-type Na$_V$1.4 and Na$_V$1.4$_{1740}$. (C) Confocal images of Na$_V$1.4-EYFP expressed in HEK293 cells. EYFP-fused wild-type channels are distributed in both the periphery and center of the cell. The right panel is a DIC image and bottom panel is the merge of the DIC and fluorescence images. (D) In contrast, Na$_V$1.4$_{IQ/AA}$ mutant channels fused to EYFP are predominantly distributed in the perinuclear region of the cell, indicating mutant channels are synthesized but remain trapped in internal membranes. The images are as described in C.

the IQ motif, the longer construct will permit binding. Both constructs exhibit robust currents when expressed in HEK293 cells (Fig. 5 A). The normalized current–voltage (Fig. 5 A) relationships of the Na$_V$1.4$_{1740}$–G4-CaM or Na$_V$1.4$_{1740}$–G14-CaM and wild-type channel are nearly identical with the peak current amplitudes at approximately −20 mV. The τ_{rec} of Na$_V$1.4$_{1740}$–G4-CaM (4.2 ± 0.2 ms, $n = 8$) is not significantly different from that of Na$_V$1.4$_{1740}$–G14-CaM (4.6 ± 0.3 ms, $n = 5$; Fig. 5 B), but both are longer than the full-length Na$_V$1.4. Similarly lengthening the glycine linker from 4 to 14 does not significantly alter τ_{entry} (Na$_V$1.4$_{1740}$–G4–CaM 700 ± 15 ms, $n = 6$, versus Na$_V$1.4$_{1740}$–G14–CaM 760 ± 10.4 ms, $n = 6$, Fig. 5 C). We then examined the voltage-dependent shift in steady-state inactivation mediated by CaM binding to the CT. The V$_{1/2}$ of the steady-state inactivation curve of Na$_V$1.4$_{1740}$–G4–CaM is −65.1 ± 0.1 mV ($n = 8$) and overexpression of ECFP-CaM with Na$_V$1.4$_{1740}$–G4–CaM shifts the V$_{1/2}$ ∼5 mV (V$_{1/2}$ −71.5 ± 0.2 mV, $n = 6$) in the hyperpolarizing direction (Fig. 5 D). Overexpression of ECFP-CaM$_{1234}$ with Na$_V$1.4$_{1740}$–G4–CaM does not shift channel availability curve compared with Na$_V$1.4$_{1740}$–G4-CaM expression alone (−63.6 ± 0.2 mV, $n = 5$; Fig. 5 D). Thus the shorter length glycine linker fused CaM to channel (Na$_V$1.4$_{1740}$–G4-CaM) retains the CaM-induced modulation of steady-state inactivation of wild-type Na$_V$1.4 channels (Table I). In contrast, lengthening the glycine linker to 14 shifts the steady-state inactivation curve of Na$_V$1.4$_{1740}$–G14-CaM in the hyperpolarizing direction (V$_{1/2}$ −68.8 ± 0.1 mV, $n = 5$) and overexpression of ECFP-CaM does not alter the voltage dependence of inactivation of Na$_V$1.4$_{1740}$–G14-CaM (V$_{1/2}$ −67.7 ± 0.2 mV, $n = 9$, Fig. 5 E). Similarly overexpression of ECFP-CaM$_{1234}$ with Na$_V$1.4$_{1740}$–G14-CaM (V$_{1/2}$ −66.7 ± 0.2 mV, $n = 9$) does not shift channel availability curve compared with Na$_V$1.4$_{1740}$–G14-CaM expression alone (Fig. 5 E). CaM linked to the channel by four glycines remained sensitive to overexpression of CaM; in contrast, CaM linked by 14 glycines was no longer sensitive to CaM overexpression, suggesting that a single CaM is sufficient for Na$_V$1.4 modulation. These data further support the role of CaM binding to the CT of Na$_V$1.4 in modulating the voltage dependence of inactivation of the channel.

Association of CaM with CT-Na$_V$1.4 Assessed by FRET

The electrophysiological data suggest that CaM is tethered to Na$_V$1.4. We coexpressed Na$_V$1.4-EYFP and ECFP-CaM and used donor dequenching FRET to study the proximity of ECFP-CaM to the CT of Na$_V$1.4. The FRET efficiency (%) using donor dequenching was computed as previously described (Erickson et al., 2001). Cells expressing ECFP alone ($n = 5$) or coexpressing ECFP with EYFP ($n = 15$) exhibited no FRET (Fig. 6 A); however, HEK293 cells expressing the linked chameleon ECFP-EYFP yield a FRET efficiency of 28.3 ± 2.8% ($n = 12$; Fig. 6 A), which is consistent with previously reported FRET results in Ca$_V$1.2 (Erickson et al., 2001). A mean FRET efficiency 10.3 ± 1.3% ($n = 22$; Fig. 6 A) was observed when ECFP-CaM was coexpressed with EYFP-tagged channels, indicating that the fluorophores in Na$_V$1.4-EYFP and ECFP-CaM were separated by <100 Å. In contrast, when the IQ residues of the CaM binding motif in

the Na$_V$-CT were substituted by alanines (Na$_v$1.4$_{IQ/AA}$), no FRET was observed between the donor ECFP-CaM and acceptor Na$_V$1.4$_{IQ/AA}$-EYFP (Fig. 6 A). Coexpressing free cytosolic ECFP with Na$_V$1.4-EYFP does not yield FRET (Fig. 6 A). The absence of FRET between the mutant IQ channel and CaM, and the wild-type channel and free cytosolic ECFP, excludes possibility of FRET due to generalized enrichment of CaM at the cell membrane, and nonspecific binding of CaM to the channel. Moreover, no FRET was evident between the CaM EF hand mutant ECFP-CaM$_{1234}$ and Na$_V$1.4-EYFP (Fig. 6 A), suggesting the absence of unconventional binding sites for apo-CaM in the intact CT of Na$_V$1.4, as has been observed in L-type Ca^{2+} channels (Erickson et al., 2001, 2003). Mutant CaM$_{1234}$ does not bind Ca^{2+} at physiological intracellular concentrations (Xia et al., 1998), suggesting that the interaction of CaM with Na$_V$1.4 under resting conditions is Ca^{2+} dependent.

To determine if channel surface expression influenced FRET efficiency, current densities of the channels were compared in the presence and absence of ECFP-CaM coexpression (Fig. 6 B; Table I). The presence of ECFP-CaM did not significantly alter the current density of any of the Na channel variants studied compared with the channel expressed alone or coexpressed with ECFP. However we caution that the cells studied were highly selected to have peak current densities in a range that allows for adequate detection and reliable voltage control.

The association of CaM with the CT of Na$_V$1.4 was tested with a complementary, nondestructive FRET measurement technique, 3^3 FRET (Erickson et al., 2001). Expression of CT-Na$_V$1.4-EYFP with ECFP-CaM resulted in a FRET ratio (FR) of >1, with a mean FRET efficiency ~8.2% (n = 12; Fig. 6 C), confirming the association of CaM to the CT-Na$_V$1.4. Consistent with the donor dequenching FRET results, the 3^3 FRs were <1 in cells expressing the Na$_V$1.4$_{IQ/AA}$ channel with CaM (Fig. 6 C). Thus FRET is the result of a specific CaM–channel interaction at the IQ motif.

To understand the mechanism of modulation of inactivation of Na$_V$1.4 we examined the voltage dependence of the interaction of CaM and its proximity to the CT fluorescent Na channel tag. We measured donor dequenching FRET between Na$_V$1.4-EYFP and ECFP-CaM while holding the channels at three different potentials: −140 mV (favoring closed channels), −60 mV (~V$_{1/2}$ of the inactivation curve), and −20 mV (favoring inactivated channels). Coexpressing ECFP-CaM and Na$_V$1.4-EYFP enhanced the ECFP signal in patch-clamped cells held at −140 mV, leading to a mean 22.7 ± 2.0% (n = 15) FRET efficiency, which is significantly (P < 0.0006) higher than the FRET efficiency of unpatched cells (Fig. 6 D). Similarly, at a holding voltage of −60 mV, a mean FRET efficiency of 25.4 ± 1.8% (n = 9) was observed (Fig. 6 D). However, holding at −20 mV yielded a FRET efficiency

(9.9 ± 2.3%, n = 15) similar to FRET of unpatched cells (Fig. 6 D). CaM does not appear to dissociate from the channel in the closed or inactivated conformations.

CaM Influences Channel Trafficking

CaM binding to the CT of Na$_V$1.4 under resting conditions and studies describing reduced current density by expressed Na$_V$ channel isoforms that have been mutated to impair CaM binding (Cormier et al., 2002; Herzog et al., 2003) suggest that CaM binding influences channel trafficking and surface expression. In addition to calmodulation of steady-state inactivation of Na$_V$1.4, we assessed whether CaM influenced channel trafficking and expression. Lysates isolated from cells expressing wild-type or mutant Na$_V$1.4$_{IQ/AA}$ channel proteins were separated on SDS-PAGE gels (Fig. 7 A) and band intensities were measured to estimate the level of total channel expression. To assess effect of CaM binding on surface expression, cells expressing wild-type or mutant Na$_V$1.4$_{IQ/AA}$ channels were labeled with membrane-impermeable biotin and purified with streptavidin beads. The band intensities of biotinylated proteins, representing cell surface expression, were normalized to the respective total channel protein expression and plotted in Fig. 7 B. The Na$_V$1.4$_{IQ/AA}$ mutant exhibits significantly (P ≤ 0.05, n = 4) reduced surface expression compared with wild-type Na$_V$1.4 and the truncation mutant distal to the IQ, Na$_V$1.4$_{1740}$ (Fig. 7 B). Truncation of Na$_V$1.4 further upstream at residue 1723 (Na$_V$1.4$_{1723}$) eliminates channel function (Fig. 4 G) but does not eliminate cell surface expression, as detected by Western blot and epifluorescence microscopy (Fig. S2, available at http://www.jgp.org/cgi/content/full/jgp.200709863/DC1). The data suggest that the CaM binding region of the intact CT of Na$_V$1.4 is essential for functional cell surface channel expression. To further examine trafficking of the IQ mutant channel, Na$_V$1.4-EYFP or Na$_V$1.4$_{IQ/AA}$-EYFP were expressed in HEK293 cells, and the cellular channel protein distribution was examined with confocal microscopy. Fluorescence from EYFP-fused wild-type channels was distributed in both the periphery and center of the cell, consistent with trafficking from perinuclear membranes to cell surface (Fig. 7 C). In contrast, signals from the Na$_V$1.4$_{IQ/AA}$-EYFP mutant channels were predominantly in the perinuclear region, indicating mutant channels are synthesized but remain trapped in intracellular membranes (Fig. 7 D). Compared with the wild-type Na$_V$1.4 channel, more Na$_V$1.4$_{IQ/AA}$ channels remain internalized, consistent with the reduced surface expression of the Na$_V$1.4$_{IQ/AA}$ protein observed in Western blot analysis (Fig. 7, A and B). Although the IQ/AA mutation interferes with cell surface trafficking of Na$_V$1.4, truncation of the CT proximal to IQ generates nonfunctional channels that are expressed on the cell surface. It is possible that the IQ/AA mutation creates a signal that mediates retention in subcellular membranes such

as the ER. This mutation-mediated retention signal is eliminated by truncation of the IQ motif (i.e., $Na_V1.4_{1723}$), resulting in normal surface membrane trafficking of nonfunctional channels. Either the IQ motif itself or CaM binding to IQ promotes a structure of this region of the CT, likely involving residues between 1723 and 1740, that is trafficked to the cell surface.

DISCUSSION

The cytoplasmic domain of the voltage gated sodium channel participates in the formation of a multiprotein complex (Abriel and Kass., 2005). Protein–protein interactions involving the CT influence the expression, membrane trafficking, subcellular localization, and gating properties of the pore-forming subunit. Mutations of the IQ motif in the CT of Na_V channels have been shown to alter slow inactivation kinetics, generate sustained current, and reduce current density (Cormier et al., 2002; Deschênes et al., 2002; Herzog et al., 2003; Kim et al., 2004). In this study we have demonstrated, that (a) CaM is bound to the CT of intact, expressed $Na_V1.4$ at the IQ motif in a conformation-independent manner and CaM is not displaced by overexpression of the EF hand mutant CaM_{1234} (Figs. 3, 5, and 6); (b) CaM binding alters the voltage dependence of steady-state inactivation (Fig. 3A); (c) the IQ region in CT-$Na_V1.4$ is indispensable for functional expression (Fig. 4); (d) only one CaM molecule is sufficient to modulate $Na_V1.4$ channel inactivation gating current (Fig. 5, D and E); and (e) mutations in CaM binding IQ motif influence $Na_V1.4$ surface channel protein expression (Fig. 7).

CaM acts as a channel subunit binding to a C-terminal IQ motif, and a calcium sensor for calcium-dependent inactivation of $Ca_V1.2$ (Peterson et al., 1999; Zuhlke et al., 1999; Erickson et al., 2001; Van Petegem et al., 2005). An homologous IQ binding domain is present in all Na_v1 sodium channel isoforms; however, CaM's interaction with Na_V channels and its functional effects appear to be isoform specific (Mori et al., 2000; Deschênes et al., 2002; Kim et al., 2004; Young and Caldwell., 2005; Choi et al., 2006). To begin to understand the isoform-specific functional effects of Ca^{2+}/CaM/CaMK on Na_V1 isoforms and the role of the IQ motif and alternate sites of CaM and apo-CaM interaction we have examined the effect of CaM binding to the CT of skeletal muscle channel, $Na_V1.4$.

CaM Is Tethered to Intact $Na_v1.4$ through an IQ Motif
Our data conclusively demonstrate tethering of CaM to the CT of intact $Na_V1.4$ channels in live cells. Deletion mutations of the $Na_V1.4$ CT that preserve the IQ motif ($Na_V1.4_{1740}$) generated currents that had voltage dependences and kinetics of activation and inactivation that were similar to wild-type $Na_V1.4$ (Fig. 4, C and F). In contrast, deletion of the entire nonstructured region and part of the terminal α-helix including the IQ motif

($Na_V1.4_{1723}$) exhibit no current (Fig. 4 G), indicating that the region containing the IQ motif and CaM binding to this motif in $Na_V1.4$ is indispensable for normal sodium channel functional expression. CaM tethering to the IQ region was further confirmed by the absence of an effect of CaM_{1234} on the CaM-induced shift in gating of $Na_V1.4$ (Fig. 3 A). In contrast, the effects of AIP290-309 (CaM anti-peptide) are more complex and independent of CaM binding to the channel at the IQ motif (Fig. 3, B–E). AIP290-309 alters the gating of wild-type and IQ/AA mutant $Na_V1.4$ channels. Inactivation of $Na_V1.4_{IQ/AA}$ is destabilized by AIP290-309 independent of the presence of CaM overexpression (Fig. S1), whereas, steady-state inactivation of $Na_V1.4$ is shifted to depolarized potentials by AIP290-309 with no effect on the IV curve or recovery from inactivation. The effects of AIP290-309 on wild-type $Na_V1.4$ gating are eliminated by overexpression of CaM (Fig. 3 B). Whether AIP290–309 interacts with the channel directly and the site(s) of that interaction remain uncertain. The effects of AIP290-309 on $Na_V1.4_{IQ/AA}$ do not appear to be the result of a general inhibition of endogenous CaM function as overexpression of CaM does not mitigate the AIP290-309–induced changes in $Na_V1.4_{IQ/AA}$ gating.

In resting cells, wild-type CaM increased the donor dequenching FRET signal in tagged, presumably inactivated $Na_V1.4$ channels (Fig. 6, A and C). Changing the membrane voltage did not eliminate FRET, suggesting that CaM is tethered to the CT of $Na_V1.4$ in all channel conformations; however, the proximity of the fluorophores may be different in channels subjected to depolarized voltages for extended periods of time (slow inactivated states). In any case, these data confirm the importance of the IQ motif in the CT for CaM binding and modulation of the voltage dependence of gating of $Na_V1.4$ channels. This is in contrast to a previously proposed mechanism of gating for voltage-gated cardiac sodium channels, $Na_V1.5$ (Shah et al., 2006), where CaM has been proposed to bind to the IQ motif at resting Ca^{2+} levels, but later dissociates from the CT upon Ca^{2+} binding, thus enabling the CaM-free IQ motif to interact with an EF hand motif in the CT of the channel. However we observed wild-type $Na_V1.4$ and mutant $Na_V1.4_{IQ/AA}$ are both regulated by Ca^{2+} in the presence of endogenous CaM (unpublished data). Moreover, CaM-mediated regulation of $Na_V1.4$ is lost in the absence of Ca^{2+}, consistent with Ca^{2+}-dependent CaM regulation of $Na_V1.4$ gating (Deschênes et al., 2002). Finally, $Na_V1.4_{IQ/AA}$ mutant channels are not regulated by CaM but retain sensitivity to Ca^{2+}, thus at least one form of Ca^{2+}-mediated regulation of channel gating does not require an interaction between the IQ motif and the EF hand. The loss of FRET between CaM and $Na_V1.4_{IQ/AA}$ and the absence of an interaction between wild-type $Na_V1.4$ and CaM_{1234} indicates that CaM-Ca^{2+} binds to the CT via the IQ motif. CaM-Ca^{2+} regulation of channel gating is

mediated principally through Ca^{2+} binding to CaM complexes with IQ in the $Na_V1.4$-CT.

A Functional Model for the Regulation of $Na_V1.4$ Channel Gating by CaM

The conformation-independent tethering of CaM to the IQ motif is central to the model presented. Additional electrophysiogical evidence supports the idea that CaM does not dissociate from the IQ motif in $Na_V1.4$. First, overexpression of CaM_{1234} does not eliminate the CaM-mediated effect on steady-state inactivation, indicating its only CaM-mediated regulation (Fig. 3 A). Second, overexpression of both CaM and CaM_{1234} shows similar regulation to that exhibited by CaM alone (Fig. 3 B), indicating that the Ca^{2+} binding–deficient CaM_{1234} does not displace CaM. Finally, among the variable length glycine–linkered CaM fused to CT only the linker length that allows CaM to reach IQ region exhibits CaM modulation of gating, indicating one CaM molecule is sufficient for regulation of inactivation (Fig. 5, D and E). Overall the data are consistent with CaM being tethered to the CT-$Na_V1.4$ during normal gating.

The IQ motifs are highly conserved across Na_V isoforms, suggesting an important functional role for these regions. It is conceivable that the cytoplasmic tail of $Na_V1.4$ exists in a disordered form under basal depolarized conditions, when subjected to more polarized voltages, the cytoplasmic tail could be more structured due to an increase in helicity, leading to an altered binding relationship of CaM and the IQ motif (Fig. 6 D). It is possible that the binding of CaM to the more structured CT facilitates interactions with other cytoplasmic domains at pore mouth that participate in and stabilize inactivation. Further structural characterization of the $Na_V1.4$-CT and its interactions with CaM are required to critically test this hypothesis and will aid in understanding the role of CaM binding in various cardiac and muscular disorders.

Role of CaM Binding in Surface Expression of $Na_V1.4$

We demonstrate that CaM participates in the modulation of cell surface expression of intact $Na_V1.4$ channels by interaction with the IQ motif similar to other channels such as KCNQ1 (Ghosh et al., 2006), SK4 channels (Joiner et al., 2001; Lee et al., 2003), and KCNQ2/Q3 potassium channels (Wen and Levitan., 2002). It has been suggested that CaM behaves as an obligate subunit of the calcium channel, $Ca_V1.2$, altering both function and expression of this α subunit. Similarly, CaM acts as an obligate subunit of some Na_V1 channels, necessary for proper folding (Kim et al., 2004). Our data reveal that mutations in the CaM binding motif reduce total and cell surface expression of $Na_V1.4$. More proximal truncations of the channel that include the IQ motif ($Na_V1.4_{1723}$, Fig. 3 G and Fig. S2) support a role for other regions of the CT of the Na channel in both function and expression. It is possible that the IQ/AA mutation

leads to defects in proper channel folding; thus the role of CaM could be in stabilization of proper channel folding and facilitating trafficking of the channel to the cell surface. CaM regulation of channel trafficking to the cell surface and its role in the early stages of channel formation could be a general phenomenon further adding to the diversity of the CaM signaling on ion channel function.

Our data demonstrate an intimate relationship between intact $Na_V1.4$ channels and CaM that influences channel gating and functional expression, and that a single CaM molecule is sufficient to regulate $Na_V1.4$ inactivation gating. In live cells, CaM is associated with CT-Na_V under resting conditions and CaM remains tethered to the CT-Na_V over a wide range of voltages, indicating no significant displacement of CaM from any channel conformation. The $Na_V1.4_{IQ/AA}$ mutant eliminates the proximity of CaM to CT-$Na_V1.4$ and reduces $Na_V1.4$ surface expression. Thus CaM is tethered to CT-$Na_V1.4$ at the IQ motif and is essential for normal inactivation gating of $Na_V1.4$, functions to stabilize channel conformation, and promotes membrane trafficking of the channel protein.

REFERENCES

Abriel, H., and R.S. Kass. 2005. Regulation of the voltage-gated cardiac sodium channel Nav1.5 by interacting proteins. *Trends Cardiovasc. Med.* 15:35–40.

Choi, J.S., A. Hudmon, S.G. Waxman, and S.D. Dib-Hajj. 2006. Calmodulin regulates current density and frequency-dependent inhibition of sodium channel Nav1.8 in DRG neurons. *J. Neurophysiol.* 96:97–108.

Cormier, J.W., I. Rivolta, M. Tateyama, A.S. Yang, and R.S. Kass. 2002. Secondary structure of the human cardiac Na^+ channel C terminus: evidence for a role of helical structures in modulation of channel inactivation. *J. Biol. Chem.* 277:9233–9241.

Deschênes, I., N. Neyroud, D. DiSilvestre, E. Marban, D.T. Yue, and G.F. Tomaselli. 2002. Isoform-specific modulation of voltage-gated Na^+ channels by calmodulin. *Circ. Res.* 90:E49–E57.

Erickson, M.G., B.A. Alseikhan, B.Z. Peterson, and D.T. Yue. 2001. Preassociation of calmodulin with voltage-gated Ca^{2+} channeis revealed by FRET in single living cells. *Neuron.* 31:973–985.

Erickson, M.G., H. Liang, M.X. Mori, and D.T. Yue. 2003. FRET two-hybrid mapping reveals function and location of L-type Ca^{2+} channel CaM preassociation. *Neuron.* 39:97–107.

Ghosh, S., D.A. Nunziato, and G.S. Pitt. 2006. KCNQ1 assembly and function is blocked by long-QT syndrome mutations that disrupt interaction with calmodulin. *Circ. Res.* 98:1048–1054.

Herzog, R.I., C. Liu, S.G. Waxman, and T.R. Cummins. 2003. Calmodulin binds to the C terminus of sodium channels Nav1.4 and Nav1.6 and differentially modulates their functional properties. *J. Neurosci.* 23:8261–8270.

Joiner, W.J., R. Khanna, L.C. Schlichter, and L.K. Kaczmarek. 2001. Calmodulin regulates assembly and trafficking of SK4/IK1 Ca^{2+}-activated K^+ channels. *J. Biol. Chem.* 276:37980–37985.

Kearney, J.A., N.W. Plummer, M.R. Smith, J. Kapur, T.R. Cummins, S.G. Waxman, A.L. Goldin, and M.H. Meisler. 2001. A gain-offunction mutation in the sodium channel gene Scn2a results in seizures and behavioral abnormalities. *Neuroscience.* 102:307–317.

Keating, M.T., and M.C. Sanguinetti. 2001. Molecular and cellular mechanisms of cardiac arrhythmias. *Cell.* 104:569–580.

Kim, J., S. Ghosh, H. Liu, M. Tateyama, R.S. Kass, and G.S. Pitt. 2004. Calmodulin mediates Ca^{2+} sensitivity of sodium channels. *J. Biol. Chem.* 279:45004–45012.

Lee, W.S., T.J. Ngo-Anh, A. Bruening-Wright, J. Maylie, and J.P. Adelman. 2003. Small conductance Ca^{2+}-activated K^+ channels and calmodulin: cell surface expression and gating. *J. Biol. Chem.* 278:25940–25946.

Lossin, C., D.W. Wang, T.H. Rhodes, C.G. Vanoye, and A.L. George Jr. 2002. Molecular basis of an inherited epilepsy. *Neuron.* 34:877–884.

Mori, M., T. Konno, T. Ozawa, M. Murata, K. Imoto, and K. Nagayama. 2000. Novel interaction of the voltage-dependent sodium channel (VDSC) with calmodulin: does VDSC acquire calmodulin-mediated Ca^{2+}-sensitivity? *Biochemistry.* 39:1316–1323.

Peterson, B.Z., C.D. DeMaria, J.P. Adelman, and D.T. Yue. 1999. Calmodulin is the Ca^{2+} sensor for Ca^{2+}-dependent inactivation of L-type calcium channels. *Neuron.* 22:549–558.

Shah, V.N., T.L. Wingo, K.L. Weiss, C.K. Williams, J.R. Balser, and W.J. Chazin. 2006. Calcium-dependent regulation of the voltage-gated sodium channel hH1: intrinsic and extrinsic sensors use a common molecular switch. *Proc. Natl. Acad. Sci. USA.* 103:3592–3597.

Van Petegem, F., F.C. Chatelain, and D.L. Minor Jr. 2005. Insights into voltage-gated calcium channel regulation from the structure of the CaV1.2 IQ domain-Ca^{2+}/calmodulin complex. *Nat. Struct. Mol. Biol.* 12:1108–1115.

Wang, G.K., C. Russell, and S.Y. Wang. 2003. State-dependent block of wild-type and inactivation-deficient Na channels by flecainide. *J. Gen. Physiol.* 122:365–374.

Wen, H., and I.B. Levitan. 2002. Calmodulin is an auxiliary subunit of KCNQ2/3 potassium channels. *J. Neurosci.* 22:7991–8001.

Wu, F.F., E. Gordon, E.P. Hoffman, and S.C. Cannon. 2005. A C-terminal skeletal muscle sodium channel mutation associated with myotonia disrupts fast inactivation. *J. Physiol.* 565:371–380.

Xia, X.M., B. Fakler, A. Rivard, G. Wayman, T. Johnson-Pais, J.E. Keen, T. Ishii, B. Hirschberg, C.T. Bond, S. Lutsenko, et al. 1998. Mechanism of calcium gating in small-conductance calcium-activated potassium channels. *Nature.* 395:503–507.

Yang, N., S. Ji, M. Zhou, L.J. Ptacek, R.L. Barchi, R. Horn, and A.L. George Jr. 1994. Sodium channel mutations in paramyotonia congenita exhibit similar biophysical phenotypes in vitro. *Proc. Natl. Acad. Sci. USA.* 91:12785–12789.

Young, K.A., and J.H. Caldwell. 2005. Modulation of skeletal and cardiac voltage-gated sodium channels by calmodulin. *J. Physiol.* 565:349–370.

Zuhlke, R.D., G.S. Pitt, K. Deisseroth, R.W. Tsien, and H. Reuter. 1999. Calmodulin supports both inactivation and facilitation of L-type calcium channels. *Nature.* 399:159–162.